



Cite this: DOI: 10.1039/d1cy00384d

β -Diketone boron difluoride dye-functionalized conjugated microporous polymers for efficient aerobic oxidative photocatalysis†

Weitao Gong,^{id}*^{ab} Kaixun Dong,^a Lu Liu,^a Mehdi Hassan^c and Guiling Ning^{*ab}

Incorporation of organic chromophores into conjugated micro/mesoporous polymers (CMPs) provides a promising avenue for developing recyclable heterogeneous photocatalysts by overcoming tedious separation and low reusability of homogeneous organic dye-based photocatalysts. However, the design principle and the underlying structure–property relationship for fabricating and selecting various organic dye-embedded CMPs for efficient photocatalysis have not been well-constructed so far. In this study, we described the rational fabrication of two new CMPs via the one-step Sonogashira coupling using β -diketone boron difluoride dye as the key linker and commonly used building blocks (triphenylamine/triphenylbenzene) as the cores. The resulting boron-dye containing CMPs were efficiently employed as the metal-free photocatalysts in two typical aerobic oxidative organic transformations including coupling of benzylamine and oxidation of aryl boronic acids to corresponding aryl phenols, which have never been explored with other boron-dye-embedded CMPs. They exhibited superior photocatalytic performance compared to their boron-free counterparts due to their wide visible-light absorption, narrow optical bandgaps, and extended π -conjugation due to boron-complexation. The present study establishes β -diketone boron difluoride dyes as efficient building blocks for fabricating new CMP-based photocatalysts.

Received 3rd March 2021,
Accepted 15th April 2021

DOI: 10.1039/d1cy00384d

rsc.li/catalysis

Introduction

Sunlight is a great source of sustainable clean energy and a good candidate for alleviating energy and environmental difficulties in the modern world.^{1–4} As a promising photochemical transformation technology driven by sunlight, artificial photocatalysis has become a research hotspot due to its renewable and environmentally benign process.^{5–8} However, the development of task-specific photocatalysts remains highly challenging. To date, numerous organometallic compounds^{9–12} and metal-free organic chromophores^{13–17} have been investigated as photocatalysts for visible-light-induced organic transformations due to their adjustable absorptive capacity for visible-light and redox potentials in excited states. However, the high cost and toxicity associated with metal-based photocatalysts and the

intrinsically low reusability for molecular organic dyes restrict their further applications. Therefore, the development of metal-free, heterogeneous photocatalysts has attracted considerable attention in recent years for resolving the disadvantages of homogeneous photocatalytic systems.^{18–20}

Conjugated micro/mesoporous polymers (CMPs), as an emerging class of porous organic materials, have arisen as an ideal platform for constructing new heterogeneous photocatalysts. Featuring their high stability, tailorable porosity, and surface properties, and diverse structural designability, CMP-type photocatalysts exhibit promoted activities and performance compared with conventional homogeneous molecular organic dyes, due to their good recyclability, efficient separation and migration of photogenerated electron–hole pairs, and effective substrate transformations.^{21–23} To achieve enhanced photocatalytic properties, implementation of organic chromophores directly into the backbone of CMPs has been deemed as an attractive strategy to fabricate photoactive CMPs. Indeed, commonly used homogeneous organic photoredox catalysts, such as phthalocyanines, isoindigo, and eosin-Y, have been recently explored as prominent building blocks for the construction of various CMPs to realize strong and broadband light absorption.^{24–26} However, as a major constituent of organic dyes, boron-based fluorophores have been largely ignored

^a State Key Laboratory of Fine Chemicals, School of Chemical Engineering, Dalian University of Technology, Dalian 116024, P. R. China. E-mail: ninggl@dlut.edu.cn

^b Engineering Laboratory of Boric and Magnesium Functional Material Preparative and Applied Technology, Dalian, Liaoning Province, 116024, P. R. China

^c Department of Chemistry, University of Baltistan, Skardu, Pakistan

† Electronic supplementary information (ESI) available: TGA curves, XRD patterns, SEM images, Mott–Schottky curves, ¹H NMR spectra and the comparison of catalytic performance with the reported catalysts. See DOI: 10.1039/d1cy00384d

and only BODIPY-type dyes have been reported as key building blocks for constructing CMPs. It is well-known that the main drawback of BODIPY dyes is their narrow Stokes shifts inducing strong self-absorption and this would restrict their light-harvesting activity. Thus, the presently reported organic transformations photocatalyzed by BODIPY-based CMPs are just limited in the oxidation of sulfides and α -terpinene.^{27–31} Therefore, the rational construction of new boron-dye-based CMP photocatalysts for expanding organic transformation is highly desired.

Among all boron-based fluorophores, the β -diketone boron difluoride complex, built around an O[−]B⁺O pattern, has recently gained much interest in fluorescence sensing and photocatalysis due to its diverse structural modification and excellent photooptical properties.^{32–35} Chelating four-coordinated B^{III} atoms to configurationally lock O, O ligands is beneficial for fine-tuning their optical properties by making the π -system more planar, thereby enhancing the charge-transfer along the main molecular axis. However, it is a pity that there is no report regarding the incorporation of β -diketone boron difluoride dyes as key building blocks into CMPs.

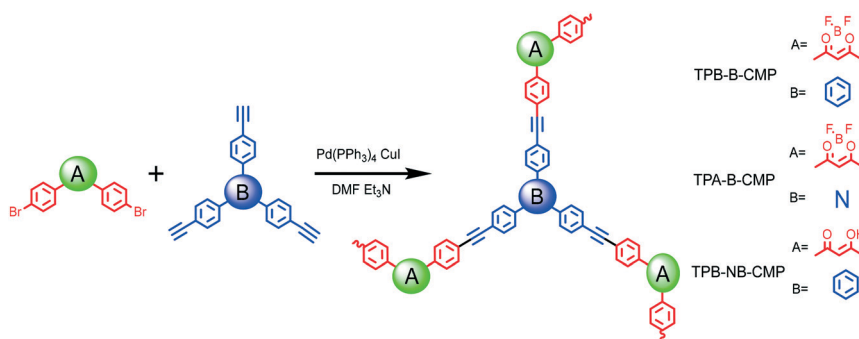
To examine the potential feasibility of new boron-dye-based CMPs as efficient photocatalysts and realize expanded photocatalytic organic transformations, in this manuscript, we designed and prepared two new boron-dye-based photoactive CMPs, named TPA-B-CMP and TPB-B-CMP *via* the one-step Sonogashira coupling using the β -diketone boron difluoride dye as the key linker and commonly selected building blocks (triphenylamine and triphenylbenzene) as the cores (Scheme 1). The as-prepared polymers were then exploited as efficient metal-free photocatalysts in two typical aerobic oxidative organic transformations including coupling of primary amines and oxidation of aryl boronic acids to corresponding aryl phenols, which have never been explored with other boron dye-embedded CMPs. TPA-B-CMP with enhanced electron donor–acceptor characteristics exhibited better photocatalytic activity than TPB-B-CMP. More significantly, because of their wide visible-light absorption, narrow optical bandgaps, and extended π -conjugation due to boron-complexation, the two boron-containing CMPs displayed superior photocatalytic performance compared to boron-free counterparts, simplified as TPB-NB-CMP, implying

the positive role of the β -diketone boron complex, which may provide new insight into designing new types of organic dye-based CMPs for photocatalytic organic transformations.

Results

Preparation and characterization of the CMPs

Selecting the same β -diketone boron difluoride dye (DBF) as the key linker and different alkynes as the cores, two boron-dye-based polymers TPA-B-CMP and TPB-B-CMP were successfully constructed through the well-developed Sonogashira–Hagihara cross-coupling reaction (Scheme 1). As for TPA-B-CMP, the introduction of a triphenylamine functional group as the core would enhance the donor–acceptor characteristics in the structure compared with TPB-B-CMP and induce different photocatalytic activities consequently. Additionally, to provide an insight into the role of β -diketone boron difluoride dye, a control polymer TPB-NB-CMP was also synthesized under similar reaction conditions. After polymerization, three polymer networks were obtained as different colorful powders, which are insoluble in most common organic solvents, such as dichloromethane (DCM), ethyl acetate (EA), acetonitrile (CH₃CN), methanol (MeOH), tetrahydrofuran (THF), and dimethyl sulfoxide (DMSO). Furthermore, they also showed excellent chemical stability after treatment of H₂O, 12 M HCl and 12 M NaOH for 3 days. The chemical structures of the as-prepared CMPs were well characterized by FT-IR and solid-state ¹³C cross-polarized NMR. As shown in Fig. 1a, the disappearance of the absorption peaks at around 3265 cm^{−1} and 3270 cm^{−1} (attributed to the characteristic stretching vibration of the H–C≡C bond on the different alkyne monomers) and the present peaks at 1482, 1367, and 1045 cm^{−1} (assigned to the characteristic bands of the β -diketone core) implied the successful polymerization. The further detailed connections were analyzed *via* solid-state ¹³C cross-polarized NMR spectroscopy. As shown in Fig. 1b, the signals related to tertiary and carbonyl carbons on the β -diketone group appeared at around 91 ppm and 181–195 ppm, respectively, according to the ¹³C NMR spectrum of model monomer DBFA (Fig. S7†). The broad range of peaks that appeared at δ 115–150 ppm is assigned to the aromatic



Scheme 1 Synthesis of TPA-B-CMP, TPB-B-CMP and TPB-NB-CMP by the Sonogashira–Hagihara cross-coupling reaction.

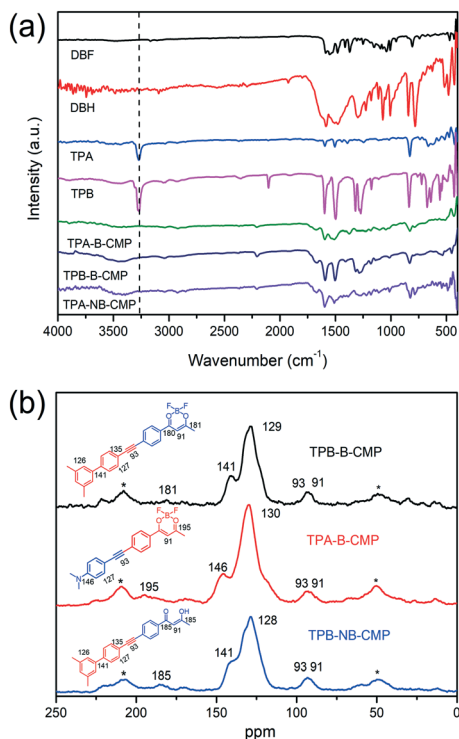


Fig. 1 (a) Fourier transform infrared (FT-IR) spectra of the monomers and TPA-B-CMP, TPB-B-CMP and TPB-NB-CMP; (b) solid-state ¹³C NMR spectra of TPB-B-CMP, TPA-B-CMP, and TPB-NB-CMP; asterisks denote the spinning sidebands.

carbon of the benzene ring and the sp-hybridized carbon of triple bonds in the phenylacetylene unit is found at around $\delta = 93$ ppm further validating the formation of the polymers. Thermogravimetric analysis (TGA) (Fig. S1†) showed that the polymers are thermally stable up to around 400 °C with less than 10% weight loss. The polymers are amorphous in nature, as indicated by the broad powder X-ray diffraction (PXRD) patterns (Fig. S2†), which could also be further proved by the irregular worm-like structure shown in the SEM images (Fig. S3†).

The permanent porosities of TPA-B-CMP, TPB-B-CMP, and TPB-NB-CMP were characterized by using N₂ adsorption-desorption measurements at 77 K (Fig. 2a). All the polymers were observed to show narrow pore size distributions centered at 2.38, 3.14, and 4.22 nm, respectively, combined with the pore size distribution profiles and nonlocal density functional

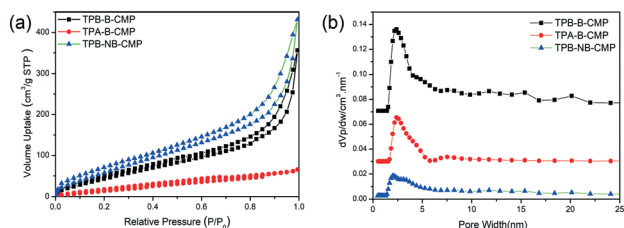


Fig. 2 (a) Nitrogen adsorption-desorption isotherms of TPA-B-CMP, TPB-B-CMP and TPB-NB-CMP at 77 K; (b) pore size distributions of TPB-B-CMP, TPA-B-CMP, and TPB-NB-CMP.

theory (Fig. 2b). The Brunauer-Emmett-Teller (BET) surface areas of TPA-B-CMP, TPB-B-CMP, and TPB-NB-CMP were calculated to be 84, 207, and 296 m² g⁻¹, respectively. Among them, TPA-B-CMP exhibited the lowest specific surface area and average pore size, possibly due to the strong π - π stacking effects between the linkers and the smaller molecular size of the triphenylamine moiety.³⁶ The SEM image of TPA-B-CMP shows fused sphere-like features, revealing that it will not have a large surface area (Fig. S3†). TPB-NB-CMP exhibited the highest specific surface area and average pore size due to the absence of coordination boron difluoride.

Photophysical properties

A close inspection of the optoelectronic properties of the three polymers and their corresponding precursors in the solid-state was initially carried out by using diffuse reflectance UV-vis spectroscopy. As shown in Fig. 3a, all the polymers displayed a broader range of absorption bands compared with their corresponding monomers indicating that the extended conjugation was realized after successful polymerization. Conspicuously, TPA-B-CMP and TPB-B-CMP exhibited an obvious red-shift compared to their control polymer TPB-NB-CMP indicating the positive role of boron complexation in their visible light absorption properties. TPA-B-CMP with an enhanced electron donor-acceptor structure showed the maximum absorption range and this result implied that the light absorption capability of the corresponding polymers can be adjusted by selecting different electron-rich coupled monomers. UV-vis experiment combined with the Kubelka-Munk equation is a commonly used method for estimating the band gap of polymers (Fig. 3b). After calculation, the optical bandgaps of TPA-B-CMP, TPB-B-CMP, and TPB-NB-CMP were determined to be

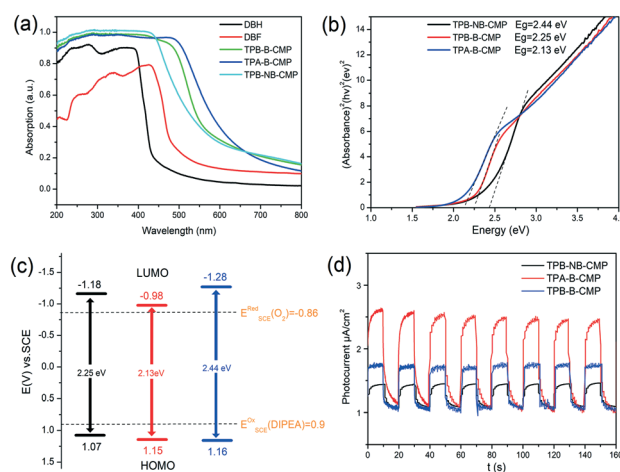


Fig. 3 (a) Normalized UV/vis absorption spectra of TPB-B-CMP, TPA-B-CMP, and TPB-NB-CMP with the corresponding monomers; (b) Kubelka-Munk-transformed reflectance spectra; (c) schematic energy band structures of TPB-B-CMP (black line), TPA-B-CMP (red line) and TPB-NB-CMP (blue line); (d) transient photocurrent response of TPB-B-CMP, TPA-B-CMP, and TPB-NB-CMP under visible-light irradiation.

2.13, 2.25, and 2.44 eV, respectively. To further determine the relative positions of the valence band (VB) and conduction band (CB), the electrochemical Mott–Schottky technique was performed. The positive slopes in the Mott–Schottky plots showed that three polymers are n-type semiconductors (Fig. S4†), and the corresponding CB potentials are -0.98 , -1.18 and -1.28 eV vs. SCE. Therefore, the position of the valence band (VB), 1.07 eV for TPA-B-CMP, 1.14 eV for TPB-B-CMP and 1.15 eV for TPB-NB-CMP, can be derived from the optical band gap (Fig. 3c). To our delight, the oxidation/reduction potentials of these polymers are sufficient to activate some molecules into their active states, for example, the oxidation potential of DIPEA at $+0.90$ V vs. SCE and the reduction potential of O_2 at -0.86 V vs. SCE, which are comparable with those of classic catalysts, such as $^*[Ru(bpy)_3]^{2+}$ (-0.81 V vs. SCE) and $[Ru(bpy)_3]^{3+}$ ($+1.29$ V vs. SCE).^{37,38} The photocurrent response signal of photocatalytic materials can effectively reflect the photogenerated carrier migration ability of the materials. As shown in Fig. 3d, TPA-B-CMP exhibits the best photocurrent response signal due to the presence of an electron-rich triphenylamine group for the enhanced electron-donating properties. This establishment of efficient donor–acceptor characteristics in the polymer skeleton may promote the charge transfer at the interface and effectively separate the photoinduced electron–hole pairs.

Photocatalytic performance studies

As mentioned previously, to date, the organic transformations photocatalyzed by boron-dye-based CMPs were just restricted in the oxidation of sulfides and α -terpinene.^{27–31} In order to evaluate the potential feasibility of new boron-dye-based CMPs as efficient photocatalysts and realize expanded photocatalytic organic transformations, two types of photocatalytic aerobic oxidation, including the oxidative coupling of amines and oxidation of aryl boronic acids to the corresponding aryl phenols were selected to screen the most efficient photocatalyst from our as-prepared boron-containing polymers. Initially, we choose the photocatalytic oxidation of primary amines to imines as the

first model transformation.^{25,39,40} To our delight, for TPA-B-CMP and TPB-B-CMP, with the presence of a small amount of catalyst (1% mmol), the reaction could reach complete conversion within 18 hours, which was highly comparable to the organic photocatalysts published previously (Table S1†). However, as a contrast, the transformation enabled by TPB-NB-CMP only afforded a low yield of 77%, highlighting the critical role of β -diketone boron difluoride dye in the polymer structure. The higher photocatalytic activity and shorter reaction time of TPA-B-CMP compared with those of TPB-B-CMP might be ascribed to the strengthened donor–acceptor structure in its skeleton and the promoted charge-transfer and separation capability. Furthermore, under the same conditions, the reaction yield using TPA-B-CMP (entry 3, Table 1) as the catalyst is 1.7 times higher than that of the molecular model catalyst (entry 6, Table 1). This result verified that the extended π -conjugated structure of TPA-B-CMP is significant for realizing efficient photocatalysis. In addition, no target product was detected in the absence of an oxygen source (entry 4), light (entry 5), or photocatalyst (entry 7) in the control experiments, implying the essential role of catalysts, oxygen, and light.

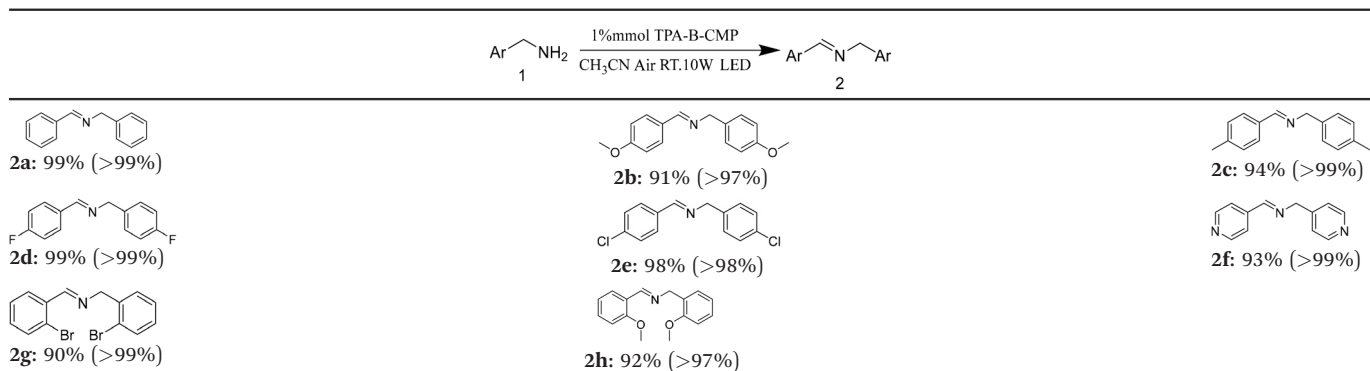
Since TPA-B-CMP exhibited the highest photocatalytic activity, we selected it as the photocatalyst to test the substrate scope of aromatic primary amines to validate the generality of TPA-B-CMP. As shown in Table 2, in the presence of TPA-B-CMP, a series of amines with different *para* substituents could be converted to imines in good to excellent yields. Generally speaking, electron-withdrawing groups are more active ($>98\%$, **2d** and **2e**), and electron-donating groups are slightly less active (**2b** and **2c**). As for amines with *ortho* substituents, a little bit lower yields were observed (**2g** and **2h**), which might be due to the steric hindrance effect.

Phenol is one of the highly economical organic raw materials and has important applications in chemistry and medicine.⁴¹ Photocatalytic oxidative hydroxylation of aryl boronic acids is an effective and green synthetic way to prepare the corresponding phenols. It has been reported that benzoxazole and benzothiadiazole-based CMPs exhibit high

Table 1 Photocatalytic oxidative coupling of amines into imines^a

Entry	Catalyst	Time (h)	Sel. ^b (%)	Yield ^b (%)
1	TPA-B-CMP	6	>99	63
2	TPA-B-CMP	12	>99	80
3	TPA-B-CMP	18	>99	99
4 ^c	TPA-B-CMP	18	>99	75
2	TPB-B-CMP	18	>99	99
3	TPB-NB-CMP	18	>99	77
4 ^d	TPA-B-CMP	18	Trace	Trace
5 ^e	TPA-B-CMP	18	n.d.	n.d.
6	DBFA	18	>99	59
7	No	18	n.d.	n.d.

^a Reaction conditions: benzylamine (0.5 mmol), photocatalyst (1 mmol%), CH_3CN (5 mL), 10 W blue LED lamp (460–465 nm), room temperature (RT). ^b Yield was determined by 1H NMR. ^c Catalyst: 0.5 mmol%. ^d No O_2 . ^e No light.

Table 2 Photocatalytic oxidative coupling of arylamines in the presence of TPA-B-CMP and the product selectivities are given in parentheses^a

^a Reaction conditions: respective primary amines (0.5 mmol), photocatalyst (1 mmol%), CH₃CN (5 mL), 10 W blue LED lamp (460–465 nm), room temperature (RT).

catalytic activity for this transformation.^{16,42–44} However, there have been no reports regarding this transformation photocatalyzed by boron-dye-based CMPs yet. Therefore, we investigated the photocatalytic performance of TPA-B-CMP, TPB-B-CMP and TPB-NB-CMP in the aerobic oxidation of aryl boronic acids to phenols (Table 3). In the presence of 2 mmol% TPB-B-CMP, air, and light, phenylboronic acid was oxidized into the corresponding phenol (entry 1, >96%) with a significant yield within 48 h. In contrast, TPB-NB-CMP showed a lower activity and TPA-B-CMP exhibited the most excellent transformation efficiency among them, which is highly comparable with the reported organic photocatalysts (Table S2†). The photocatalysis factors including the sacrificial agents, oxygen, and light that may influence this transformation were systematically assessed. As shown in Table 3, when the reaction is performed in the dark or an N₂ atmosphere, it hardly proceeds (entries 4–6). In particular, the presence of a sacrificial agent is essential for the oxidation reaction of phenylboronic acid. When TPA-B-CMP was replaced with a structural monomer, the yield was only 57% after 48 hours of reaction (entry 7). It can be concluded that the photocatalytic properties of TPA-B-CMP are not only derived from the β-diketone boron difluoride moiety but also related to the π-conjugated framework.

The substrate scope was also explored by using TPA-B-CMP as the photocatalyst. Excellent reaction yields were obtained for different derivatives of boronic acid validating the generality of TPA-B-CMP (Table 4). Various aryl boronic acids, bearing either electron-donating groups such as methoxy (**4e**) and phenanthrene (**4g**) or electron-withdrawing groups such as bromide (**4b**) and carboxyl (**4c**), were effectively oxidized into the corresponding products in good to excellent yields. Notably, in general, substrates with electron-withdrawing groups have better reaction efficiencies than those with electron-donating groups.

Photocatalytic mechanism

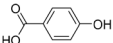
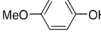
The elucidation of the plausible photocatalytic mechanism for both reactions was then conducted. It is acceptable that reactive oxygen species (ROS), like superoxide radicals (O₂^{•−}) and singlet oxygen (¹O₂), are indispensable in photocatalytic aerobic oxidative transformations.^{45,46} Therefore, the competence of TPA-B-CMP, TPB-B-CMP and TPB-NB-CMP to produce ¹O₂ and O₂^{•−} was examined initially. As shown in Fig. 4a, all the excited photocatalysts can effectively promote the generation of a purple colored 1,4-bis(dimethylamino) benzene-cationic radical and O₂^{•−}. The highest absorption

Table 3 Photocatalytic oxidation of phenylboronic acid to phenol^a

Entry	Catalyst	Time (h)	Yield ^b (%)
1	TPB-B-CMP	48	96
2	TPA-B-CMP	48	99
3	TPB-NB-CMP	48	72
4 ^c	TPA-B-CMP	48	8
5 ^d	TPA-B-CMP	48	Trace
6 ^e	TPA-B-CMP	48	n.d.
7	DBFA	48	57
8	No	48	n.d.

^a Reaction conditions: phenylboronic acid (0.5 mmol), photocatalyst (2 mmol%), DMF (5 mL), air, 10 W blue LED lamp (460–465 nm), room temperature (RT), 48 h. ^b Yield was determined by ¹H NMR. ^c No iPr₂EtN. ^d No O₂. ^e No light.

Table 4 Photocatalytic oxidative arylboronic acid hydroxylation in the presence of TPA-B-CMP^a

$\text{Ar}-\text{B}(\text{OH})_2 \xrightarrow[\text{DMF, 10W Blue LED}]{2\% \text{ mmol } i\text{Pr}_2\text{NEt, RT}} \text{Ar}-\text{OH}$		
3		4
 4a: 99%	 4b: 98%	 4c: 99%
 4d: 94%	 4e: 92%	 4f: 98%
 4g: 95%		

^a Reaction conditions: respective arylboronic acids (0.5 mmol), photocatalyst (2 mmol%), DMF (5 mL), air, 10 W blue LED lamp (460–465 nm), room temperature (RT), 48 h.

peak intensity and the deepest solution color implied that TPA-B-CMP has the superior photocatalytic activity to produce $\text{O}_2^{\cdot-}$ among the three polymers. Then, the $^1\text{O}_2$ production capacity of the photocatalysts was experimentally validated by electron paramagnetic resonance (EPR) spectroscopy using 2,2,6,6-tetramethylpiperidine (TEMP) as a spin-trapping agent for $^1\text{O}_2$. As shown in Fig. 4b, upon exposure to light, all the photocatalysts produce the characteristic 1 : 1 : 1 triplet signal due to the formation of the 2,2,6,6-tetramethylpiperidine 1-oxyl (TEMPO) radical by the reaction of TEMP with $^1\text{O}_2$. The highest strength of the EPR signal indicated that TPA-B-CMP has the best ability to activate oxygen to produce $^1\text{O}_2$.

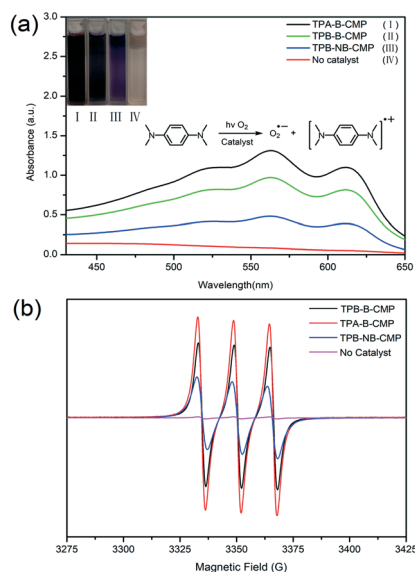


Fig. 4 (a) UV-vis absorption spectra and photographs of NTPD in acetonitrile in the presence and the absence of TPB-B-CMP, TPA-B-CMP, and TPB-NB-CMP upon irradiation by visible light (10 W blue LED); (b) the EPR spectra of TPA-B-CMP in the presence of air and TEMP after visible light irradiation.

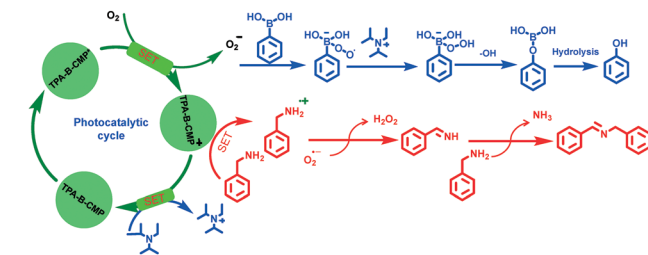


Fig. 5 Proposed mechanism for the photocatalytic transformation of primary amine by oxidative coupling (red line) and aryl boronic acids (blue line) to phenols in the presence of TPA-B-CMP.

With all the above results in hand, the plausible reaction mechanisms for both transformations were proposed, respectively (Fig. 4, Table S3[†]). Firstly, TPA-B-CMP generates TPA-B-CMP* in a photocatalytic cycle under visible light irradiation. Subsequently, excited TPA-B-CMP* can activate O_2 via a single electron transfer (SET) process and yielding $\text{O}_2^{\cdot-}$. The imines and sacrificial agents are oxidized by TPA-B-CMP* to form free radical cations while TPA-B-CMP is regenerated in a photocatalytic cycle. Superoxide radicals then extract protons from the primary amine cations, thereby producing amine intermediates and hydrogen peroxide. The imine is further reacted with the free amine to complete the coupling reaction after the removal of ammonia. The oxidation mechanism of aryl boronic acid is similar to that of primary amine oxidation. DIPEA is oxidized by losing an electron to the photogenerated hole in the excited state of TPA-B-CMP. Simultaneously, aryl boronic acid reacts with $\text{O}_2^{\cdot-}$ to form the peroxide radical as an intermediate. These intermediates obtain a proton from $\text{DIPEA}^{\cdot+}$ and lose $-\text{OH}^-$ to form intermediate peroxides, which are further rearranged and hydrolyzed into phenols (Fig. 5).

Recyclability and stability

Finally, reusability is a key factor to evaluate the potential application of a photocatalyst. Therefore, TPA-B-CMP was selected as a representative to test the recyclability in the two reactions. In each reaction, the photocatalyst TPA-B-CMP was

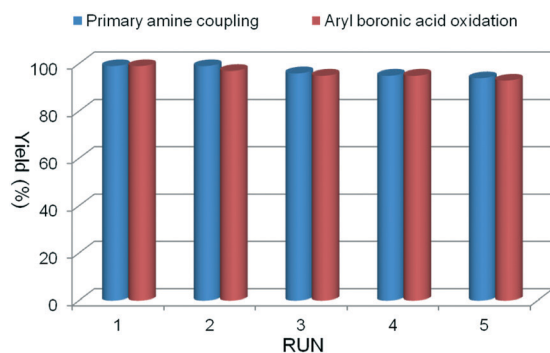


Fig. 6 Recyclability of TPA-B-CMP in primary amine coupling and aryl boronic acid oxidation. The reaction time was fixed for each cycle.

simply isolated from the reaction mixtures through centrifugation then washed, dried, and utilized in the next run of the model reaction. Five repeated experiments were performed by using the same TPA-B-CMP catalyst mostly retaining high catalytic efficiency and selectivity. The oxidative coupling of benzylamine and the oxidative conversion of phenylboronic acid can still reach 95% and 94%, respectively (Fig. 6). The chemical stability of TPA-B-CMP was also investigated by FT-IR spectroscopy (Fig. S6†). The recovered TPA-B-CMP did not show significant change compared with the original sample, indicating that the basic structure and morphology of TPA-B-CMP are still retained after photocatalysis, except the particle profile became smaller. The average 1% and 1.2% reduction in the conversion per run can be attributed to the photobleaching of the polymer or partial deactivation of superoxide radicals.

Conclusions

Two new boron-containing CMPs, TPA-B-CMP and TPB-B-CMP with β -diketone-boron difluoride dye as the key building block, were successfully prepared and exploited as efficient metal-free heterogeneous photocatalysts for aerobic oxidation of amines to imines and aryl boronic acids to phenols for the first time. They were found to be well capable of generating both singlet oxygen and superoxide anion radicals under visible-light irradiation compared to their constituent precursors and reference polymer (TPB-NB-CMP) without boron complexation. The bandgaps, energy levels, and the photocurrent response of both boron-containing CMPs were conveniently tuned simply by the implementation of enhanced donor-acceptor properties in the framework. The introduction of an electron-rich triphenylamine moiety into TPA-B-CMP can induce better visible-light adsorption and accelerated charge transfer at the interface giving rise to the best photocatalytic activity. Furthermore, as a representative photocatalyst, TPA-B-CMP displayed extensive substrate adaptability and excellent recyclability for both photocatalytic aerobic oxidation reactions. The current work provides a new insight on developing various boron-based dye incorporated CMPs as efficient photocatalysts and relative work is still ongoing in our lab.

Experimental section

Materials

All required chemicals were obtained from commercial suppliers unless otherwise specified. 4-Bromoacetophenone, methyl 4-bromobenzoate, and deuterated solvents for NMR measurement were purchased from Aladdin Chemical Reagent. Boron(III) fluoride ethylether complex (98%) and sodium hydride 60% dispersion in mineral oil were obtained from Energy Chemical. Organic solvents for reactions were purified by published standard methods. The monomers 1,3,5-tris-(4-ethynylphenyl)benzene and 1,3,5-tris(4-

ethynylphenyl)amine were synthesized according to the reported synthetic methods.⁴⁷

General procedure for the preparation of CMPs

The one-step Sonogashira coupling reactions were employed to fabricate TPA-B-CMP, TPB-B-CMP and TPB-NB-CMP.⁴⁸ In a typical procedure, monomer DBF or DBH with a dibromide group (0.75 mmol), respective alkynes (0.5 mmol), Pd(PPh₃)₄ (60 mg, 0.052 mmol), and CuI (30 mg, 0.16 mmol) were added to a 50 mL flame-dried Schlenk tube with mixed dry *N,N*-dimethyl formamide (DMF) (5 mL) and triethylamine (5 mL). The reaction suspension was degassed and then stirred at 100 °C for 3 days in an inert nitrogen atmosphere. After cooling to room temperature, the solid was obtained by filtration and washed with DMF, water, trichloromethane, methanol, and acetone. Further purification was carried out by Soxhlet extraction with methanol and trichloromethane successively for 24 h each. Finally, the solid was stirred in a tetrahydrofuran (THF)/water (1:1 v/v) solution with excess KCN to remove Pd(0). The product was then dried under a vacuum for 24 h at 60 °C to obtain the polymers as solids with different colors. The synthetic details for all compounds are given in the ESI.†

Instruments and methods

¹H NMR spectra were recorded using a Bruker Avance II 400 instrument with CDCl₃, DMSO-*d*₆, and CD₃CN as solvents, where chemical shifts (δ in ppm) were determined with a residual proton of the solvent as a standard. Fourier transform infrared (FTIR) analysis was performed by using a JASCO IR-4100 spectrometer from 400 to 4000 cm⁻¹. Solid-state ¹³C CP/MAS (cross-polarization with magic angle spinning) spectra were obtained on an Agilent DD2-500 MHz nuclear magnetic resonance spectrometer. UV-vis studies were conducted on a Hitachi UV-4100 spectrometer at room temperature. X-ray diffraction (XRD) measurements were carried out on a Rigaku D/max-2400 diffractometer by depositing the powders on a glass substrate, from $2\theta = 2^\circ$ to 40° with a scanning rate of 2° min^{-1} at 25 °C. Field emission scanning electron microscopy (FE-SEM) studies were conducted by using an FEI Nova NanoSEM 450 scanning electron microscope at 20 kV. Nitrogen sorption isotherms were measured at 77 K with a Quantachrome Autosorb iQ analyzer. Before measurement, the samples were degassed in a vacuum at 120 °C overnight. Thermogravimetric analysis (TGA) was performed by using a Mettler Toledo TGA/DSC 3+ thermal analyzer in an atmosphere of flowing N₂. All the samples were heated at room temperature to 800 °C at a heating rate of $10^\circ \text{ C min}^{-1}$. The EPR spectra were recorded on a Bruker A200-9.5/12 EPR spectrometer. The samples were quantitatively injected into 0.5 mm quartz capillaries for EPR analysis. The data of the TEMP solution with a concentration of 0.1 M was collected.

Photoelectrochemical measurement

The photoelectrochemical properties of the photocatalysts were studied on a CHI 760E electrochemical workstation using a standard three-electrode system. The working electrode was prepared with the following procedure: 5 mg photocatalyst powder and 5% Nafion were mixed in 1 mL of ethanol and sonicated for 1 h. The mixture was dripped onto a fluorine-doped tin oxide (FTO) glass ($10 \times 10 \text{ mm}^2$), and the solvent was evaporated in a vacuum chamber for 1 h to obtain the working electrode. The Mott-Schottky analysis was performed using a homemade sample electrode on FTO conductive glass as the working electrode, a platinum wire electrode as the counter electrode, and a saturated calomel electrode (SCE) as the reference electrode, measured at different frequencies. The photocurrent responses of the polymers were measured in 0.1 M Na_2SO_4 under the irradiation of a 300 W Xe lamp with 10s light on-off cycles.

Typical procedure for photocatalytic primary amine coupling

The photocatalysts (0.005 mmol), corresponding amine (0.5 mmol), and acetonitrile (5 ml) were mixed in a quartz reaction tube. The mixture was stirred under the irradiation of a WP-TEC-1020HSL photochemical reaction system with a blue LED lamp (10 W) at room temperature. Thin layer chromatography (TLC) was used to monitor the progress of the reaction. After the reactants were consumed as indicated by TLC, the reaction solid was removed by centrifugation and washed several times with CH_3CN . The supernatants were combined and dried under a vacuum. ^1H NMR was performed for the crude product in CDCl_3 , and dibromomethane was added as an internal standard to calculate the yield. The integrated peak of the product and by-product was used to calculate the selectivity. The ^1H NMR spectra of the products are consistent with the literature values.

Typical procedure for photocatalytic aryl boronic acid hydroxylation

The photocatalysts (0.01 mmol), aryl boronic acids (0.5 mmol), $i\text{Pr}_2\text{EtN}$ (1 mmol), and DMF (5 ml) were mixed in a quartz reaction tube. The mixture was stirred under the irradiation of a WP-TEC-1020HSL photochemical reaction system with the blue LED lamp (10 W) for 48 h at room temperature. The reaction was quenched with an aqueous solution of HCl (6 mL, 10%) and the solid was recovered by filtration. The filtrate was extracted with diethyl ether or ethyl acetate ($3 \times 15 \text{ mL}$). The combined organic phase was washed with a brine solution (30 mL) and dried over MgSO_4 . After concentration *in vacuo*, the solution of the concentrate was subjected to ^1H NMR analysis using $\text{DMSO}-d_6$ as the solvent, and the reaction yield was determined by the ratio between the integrated peaks of the product and substrate.⁴⁴

Author contributions

W. Gong conceived and designed the experiments. K. Dong completed the synthesis. K. Dong, M. Hassan, L. Liu, and W. Gong analyzed the data and wrote the manuscript. All the authors discussed the results and commented on and proofread the manuscript. All the authors have given approval to the final version of the manuscript.

Conflicts of interest

There are no conflicts to declare.

Acknowledgements

We are grateful for financial support from the Natural Science Foundation of Liaoning Province (No. 2019-MS-046), the Open Funds of the State Key Laboratory of Rare Earth Resource Utilization (No. RERU2020004) and the National Natural Science Foundation of China (No. U1808210).

Notes and references

- D. M. Schultz and T. P. Yoon, *Science*, 2014, **343**, 1239176–1239183.
- S. Furukawa, Y. Ohno, T. Shishido, K. Teramura and T. Tanaka, *ACS Catal.*, 2011, **1**, 1150–1153.
- X. Li, J. Xie, C. Jiang, J. Yu and P. Zhang, *Front. Environ. Sci. Eng.*, 2018, **12**, 1–32.
- Q. Wang, J. Huang, H. Sun, K. Q. Zhang and Y. Lai, *Nanoscale*, 2017, **9**, 16046–16058.
- M. Majek and A. Jacobi von Wangelin, *Acc. Chem. Res.*, 2016, **49**, 2316–2327.
- X. Lang, X. Chen and J. Zhao, *Chem. Soc. Rev.*, 2014, **43**, 473–486.
- J. M. Narayanam and C. R. Stephenson, *Chem. Soc. Rev.*, 2011, **40**, 102–113.
- N. A. Romero and D. A. Nicewicz, *Chem. Rev.*, 2016, **116**, 10075–10166.
- Z. Zhang, X. Tang and W. R. Dolbier, Jr., *Org. Lett.*, 2015, **17**, 4401–4403.
- H. Jiang, Y. Cheng, R. Wang, M. Zheng, Y. Zhang and S. Yu, *Angew. Chem., Int. Ed.*, 2013, **52**, 13289–13292.
- C. K. Prier, D. A. Rankic and D. W. MacMillan, *Chem. Rev.*, 2013, **113**, 5322–5363.
- T. Suzuki, *Chem. Rev.*, 2011, **111**, 1825–1845.
- Y. Zhi, S. Ma, H. Xia, Y. Zhang, Z. Shi, Y. Mu and X. Liu, *Appl. Catal., B*, 2019, **244**, 36–44.
- J. H. Ko, N. Kang, N. Park, H.-W. Shin, S. Kang, S. M. Lee, H. J. Kim, T. K. Ahn and S. U. Son, *ACS Macro Lett.*, 2015, **4**, 669–672.
- K. Zhang, D. Kopetzki, P. H. Seeberger, M. Antonietti and F. Vilela, *Angew. Chem., Int. Ed.*, 2013, **52**, 1432–1436.
- P. F. Wei, M. Z. Qi, Z. P. Wang, S. Y. Ding, W. Yu, Q. Liu, L. K. Wang, H. Z. Wang, W. K. An and W. Wang, *J. Am. Chem. Soc.*, 2018, **140**, 4623–4631.
- Y. Zhi, K. Li, H. Xia, M. Xue, Y. Mu and X. Liu, *J. Mater. Chem. A*, 2017, **5**, 8697–8704.

- 18 J. Byun and K. A. I. Zhang, *Mater. Horiz.*, 2020, **7**, 15–31.
- 19 J. Lin, Z. Guo and H. Zhan, *J. Catal.*, 2020, **385**, 338–344.
- 20 Z. Li, Y. Zhi, P. Shao, H. Xia, G. Li, X. Feng, X. Chen, Z. Shi and X. Liu, *Appl. Catal., B*, 2019, **245**, 334–342.
- 21 C. Dai and B. Liu, *Energy Environ. Sci.*, 2020, **13**, 24–52.
- 22 Y. Yang, H. Niu, L. Xu, H. Zhang and Y. Cai, *Appl. Catal., B*, 2020, **269**, 118799–118805.
- 23 J. Yu, X. Sun, X. Xu, C. Zhang and X. He, *Appl. Catal., B*, 2019, **257**, 117935–117943.
- 24 W.-L. He and C.-D. Wu, *Appl. Catal., B*, 2018, **234**, 290–295.
- 25 R. Chen, J. L. Shi, Y. Ma, G. Lin, X. Lang and C. Wang, *Angew. Chem., Int. Ed.*, 2019, **58**, 6430–6434.
- 26 A. Sridhar, R. Rangasamy and M. Selvaraj, *New J. Chem.*, 2019, **43**, 17974–17979.
- 27 S. Bandyopadhyay, S. Kundu, A. Giri and A. Patra, *Chem. Commun.*, 2018, **54**, 9123–9126.
- 28 M. Liras, M. Iglesias and F. Sánchez, *Macromolecules*, 2016, **49**, 1666–1673.
- 29 M. Liras, M. Pintado-Sierra, M. Iglesias and F. Sánchez, *J. Mater. Chem. A*, 2016, **4**, 17274–17278.
- 30 J. M. Tobin, J. Liu, H. Hayes, M. Demleitner, D. Ellis, V. Arrighi, Z. Xu and F. Vilela, *Polym. Chem.*, 2016, **7**, 6662–6670.
- 31 C. G. López-Calixto, S. Cabrera, R. Pérez-Ruiz, M. Barawi, J. Alemán, V. A. de la Peña O'Shea and M. Liras, *Appl. Catal., B*, 2019, **258**, 117933–117941.
- 32 W. Liu, S. Wu, Q. Su, B. Guo, P. Ju, G. Li and Q. Wu, *J. Mater. Sci.*, 2018, **54**, 1205–1212.
- 33 P.-Z. Chen, H. Zhang, L.-Y. Niu, Y. Zhang, Y.-Z. Chen, H.-B. Fu and Q.-Z. Yang, *Adv. Funct. Mater.*, 2017, **27**, 1700332–1700341.
- 34 P. Z. Chen, Y. X. Weng, L. Y. Niu, Y. Z. Chen, L. Z. Wu, C. H. Tung and Q. Z. Yang, *Angew. Chem., Int. Ed.*, 2016, **55**, 2759–2763.
- 35 Y. Kitagawa, R. Yachi, T. Nakanishi, K. Fushimi and Y. Hasegawa, *J. Phys. Chem. A*, 2017, **121**, 4613–4618.
- 36 R. Li, Z. J. Wang, L. Wang, B. C. Ma, S. Ghasimi, H. Lu, K. Landfester and K. A. I. Zhang, *ACS Catal.*, 2016, **6**, 1113–1121.
- 37 W. Huang, B. C. Ma, H. Lu, R. Li, L. Wang, K. Landfester and K. A. I. Zhang, *ACS Catal.*, 2017, **7**, 5438–5442.
- 38 C. Ayed, L. Caire da Silva, D. Wang and K. A. I. Zhang, *J. Mater. Chem. A*, 2018, **6**, 22145–22151.
- 39 X.-X. Guo, J. Jiang, Q. Han, X.-H. Liu, X.-T. Zhou and H.-B. Ji, *Appl. Catal., A*, 2020, **590**, 117352–117357.
- 40 C. Su, R. Tandiana, B. Tian, A. Sengupta, W. Tang, J. Su and K. P. Loh, *ACS Catal.*, 2016, **6**, 3594–3599.
- 41 S. Quideau, D. Deffieux, C. Douat-Casassus and L. Pouysegu, *Angew. Chem., Int. Ed.*, 2011, **50**, 586–621.
- 42 Z. J. Wang, R. Li, K. Landfester and K. A. I. Zhang, *Polymer*, 2017, **126**, 291–295.
- 43 X. Yan, H. Liu, Y. Li, W. Chen, T. Zhang, Z. Zhao, G. Xing and L. Chen, *Macromolecules*, 2019, **52**, 7977–7983.
- 44 H.-P. Liang, Q. Chen and B.-H. Han, *ACS Catal.*, 2018, **8**, 5313–5322.
- 45 S. M. Bonesi, I. Manet, M. Freccero, M. Fagnoni and A. Albin, *Chem. – Eur. J.*, 2006, **12**, 4844–4857.
- 46 J. Luo, J. Lu and J. Zhang, *J. Mater. Chem. A*, 2018, **6**, 15154–15161.
- 47 Z. Xie, Y. Wei, X. Zhao, Y. Li, S. Ding and L. Chen, *Mater. Chem. Front.*, 2017, **1**, 867–872.
- 48 S. Ren, R. Dawson, A. Laybourn, J.-X. Jiang, Y. Khimyak, D. J. Adams and A. I. Cooper, *Polym. Chem.*, 2012, **3**, 928–934.